Research Square

Preprints are preliminary reports that have not undergone peer review.
They should not be considered conclusive, used to inform clinical practice,
or referenced by the media as validated information.

Harnessing association and transcriptome analyses to prioritize novel candidate genes for maize root architecture

Mingye Zeng
Yao Miao
Yangjing Li
Jiyi Xiao
Yi Cheng
Yong Xie
Zhonghua Peng
Yulin Jiang
Xun Wu
Qiang Yi
yiqiang990@hotmail.com

Guizhou University https://orcid.org/0000-0003-2034-388X

Huidan Mo
Xianbin Hou

Research Article

Keywords: maize, root system, genome-wide association analysis, RNA-seq, candidate genes

Posted Date: November 25th, 2026

DOI: https://doi.org/10.21203/rs.3.rs-11729799/v1

License: This work is licensed under a Creative Commons Attribution 4.0 International License.
Read Full License

Additional Declarations:
Tables are available in the Supplementary Files section.

Figures are available in the Supplementary Files section.

Harnessing association and transcriptome analyses to prioritize novel candidate genes for maize root architecture

Mingye Zeng[1†], Yao Miao[1†], Yangjing Li[1†], Jiyi Xiao[1], Yi Cheng[1], Yong Xie[1], Zhonghua Peng[1], Yulin Jiang[2,3], Xun Wu[2,3], Qiang Yi[1*], Huidan Mo[4*], Xianbin Hou[4*]

[1] Guizhou Key Laboratory of High Quality, High Efficiency, and Yield Enhancement in Grain and Oil Crops, and Maize Research Institute of College of Agriculture, Guizhou University, Guiyang, 550025, China

[2] Institute of Upland Food Crops, Guizhou Academy of Agricultural Sciences, Guiyang, 550000, China

[3] Ministry of Agriculture and Rural Affairs Key Laboratory of Crop Genetic Resources and Germplasm Innovation in Karst Region, Guiyang, 550000, China

[4] College of Agriculture and Food Engineering, Baise University, Baise 533000, China

† Co-first author: these authors contributed equally

* Co-correspondence: Qiang Yi (yiqiang990@hotmail.com), Huidan Mo (1581806278@qq.com), Xianbin Hou (741623924@qq.com)

Abstract

Background and aims Roots are key organs for water and nutrient uptake in maize, a typical fibrous-root crop, but root sampling and phenotyping are difficult, particularly in the clayey soils of Southwest China. We dissected the genetic basis of maize root architecture to identify key loci and genes.

Methods Seven root traits were measured in 241 diverse maize inbred lines comprising 945 adult individuals. Genome-wide association analysis (GWAS) was performed using high-density single nucleotide polymorphism (SNP) markers, and GWAS-derived candidate genes were integrated with root RNA-seq data from two deep-root inbred lines (CIMBL111 and CML171) and one shallow-root inbred line (IBC2).

Results Seven root traits differed significantly among genotypes. These root traits showed correlations to varying degrees, among which root area was highly positively correlated with total projected structure length, and the number of first-layer roots was significantly positively correlated with the number of second-layer roots. GWAS detected 24 quantitative trait loci (QTL) comprising 73 significant SNPs, mainly distributed on chromosomes 1, 3, 5, 6, 7, 8, and 9. Kyoto Encyclopedia of Genes and Genomes (KEGG) enrichment of 12,342 differentially expressed genes (DEGs) highlighted phenylpropanoid biosynthesis, starch and sucrose metabolism, and glutathione metabolism. Integrating 280 GWAS-derived candidate genes with these DEGs yielded 62 common candidates. Combining two major-effect loci with qPCR validation prioritized three key genes: Zm00001d037968, Zm00001d037969, and Zm00001d046136.

Conclusions These loci and candidate genes provide a basis for functional validation and molecular breeding of maize root traits adapted to challenging soils.

Keywords: maize; root system; genome-wide association analysis; RNA-seq; candidate genes

Introduction

Roots are key organs for water and nutrient uptake and plant anchorage in maize, and root architecture and physiological functions play indispensable roles in plant vigor, stress resistance, and final yield (Hochholdinger 2009). Maize has a fibrous root system composed of primary roots, seminal roots, and shoot-borne roots. Seminal and shoot-borne roots are the main components for nutrient and water uptake, and their number, spatial distribution, and contact area with soil directly affect lodging resistance, nutrient use efficiency, and adaptation to stresses such as drought and poor soil fertility (Jing et al. 2022; Stamp and Kiel 1992; Zhan et al. 2015). Root architecture-related traits are typical complex quantitative traits controlled by multiple minor-effect genes and are easily affected by the environment, making genetic dissection difficult (Bray and Topp 2018). In addition, extreme weather events such as drought and flooding caused by global climate change have further intensified land degradation (IPCC, 2019), posing a serious threat to maize production in mountainous areas. Southwest China is the third largest maize production region in China, dominated by mountains and hills, with shallow effective cultivated soil layers (Chen 2024), soil compaction, poor fertility, and poor water and fertilizer retention; moreover, rainfall is highly unevenly distributed among seasons (Wei et al. 2026), leading to frequent seasonal drought and low-temperature stress. Under this special ecological condition, maize root architecture directly determines the efficiency of acquisition of limited water and nutrient resources and adaptability to stress. However, research on the genetic basis of maize root architecture under poor soil conditions in Southwest China is limited, and mining key genes and loci for adaptive root traits in this region is particularly urgent.

At present, a large number of literature regarding maize roots have mainly relied on linkage and association analysis to identify loci controlling root number, root length, root angle, and other root architecture traits (Lebreton et al. 1995; Li et al. 2020, 2023, 2024; Ren et al. 2022; Salvi et al. 2016; Wu et al. 2022) used 81 families of an F_2 population derived from P0lj × F-2 for QTL mapping of primary seminal root number, nodal root number, and root pulling force, and detected 4, 4, and 7 QTL, respectively. Salvi et al. (2016)identified three quantitative trait loci (QTL) controlling seminal root number in chromosomal regions

1.02, 3.07, and 8.04–8.05, two of which co-localized with the key root development genes *RTCS* and *rum1*. Li et al. (2020)used a recombinant inbred line (RIL) population of 208 families derived from T877 and DH1M and detected 25 QTL associated with crown root angle, crown root diameter, and crown root number in three field trials. Li et al. (2023) used 373 maize inbred lines under well-watered and drought-stress conditions and detected 221 association loci for 13 root traits by genome-wide association analysis (GWAS); among 75 strong candidate genes, *ZmCIPK3* may enhance drought tolerance. Wu et al. (2022) used an association panel of 421 maize inbred lines at the mature stage and detected 63 SNPs and 189 candidate genes, identifying four high-confidence candidate genes for root architecture. Ren et al. (2022) used an association mapping panel comprising 14,301 field-grown plants from 380 inbred lines and identified 81 high-confidence root architecture-associated candidate genes by GWAS, and found that modern breeding has selected a steep root angle. Li et al. (2024) used 513 inbred lines and four RIL populations in multiple field trials and detected 389 and 344 QTL associated with 14 shoot-borne root traits by GWAS and linkage analysis, respectively. In addition, multi-omics (Fang et al. 2024), single-cell sequencing (Wang et al. 2025), and high-throughput phenotyping and machine learning (Guo et al. 2025) have been used to reveal the relationships between root development and nitrogen-efficient utilization and high-temperature tolerance. In summary, existing studies have mostly focused on maize seedling roots or genetic dissection of root architecture in the main production region of the Huang-Huai-Hai Plain in China, whereas studies on mature-stage roots of tropical maize materials under poor soil conditions in Southwest China or karst regions remain scarce. Therefore, it is urgent to mine genetic loci related to maize root architecture under such environments.

To date, previous studies have screened and identified root mutants affecting maize seedling root length, lateral roots, and root hairs from large-scale mutagenized mutant F_2 populations, such as *Rt1*(Emerson RA et al. 1935), *rtcs* (Hetz et al. 1996; Taramino et al. 2007), *rum1* (Woll et al. 2005), *Irt1* (Hochholdinger and Feix 1998), *slr1* and *slr2* (Hochholdinger et al. 2001), and *rth1*, *rth2*, and *rth3* (Wen and Schnable 1994). Schneider et al. (2022) reported that *ZmCIPK15*, obtained by GWAS, can change the root angle at specific maize nodal positions by approximately 10°.Ren et al. (2022) validated that two auxin-related genes, *ZmRSA3.1* and *ZmRSA3.2*, participate in regulating maize root angle and root depth. He et al. (2023) mined 16 candidate genes through co-expression network analysis based on public maize root data and found that *ZmPYK2*-overexpressing lines significantly reduced root angle and enhanced gravitropism. Schneider et al. (2023) used anatomics combined with GWAS in 436 maize inbred lines and identified *bHLH121*, which regulates root cortical aerenchyma formation; functional validation showed that it regulates root cortical aerenchyma formation and thereby affects root soil resource acquisition. Zhang et al. (2026) used GWAS in 307 inbred lines grown under hydroponic conditions to detect genetic variation associated with primary root length, identified the heat shock protein-encoding candidate gene *ZmHSP20-5*, and combined mutant validation to show that this gene regulates primary root and lateral root growth, thereby affecting maize root architecture and drought tolerance.Li et al. (2025) integrated transcriptome-wide association analysis and single-cell RNA sequencing data and identified *ZmbZIP89* as an important regulator of lateral root elongation. The above genes jointly participate in the establishment of maize root architecture and affect water and nutrient uptake and stress resistance by regulating root angle and depth, gravitropism, root cortical aerenchyma formation, primary/lateral root growth, and lateral root elongation. These studies indicate that important breakthroughs have been made in the genetic regulation of maize root architecture, but as a quantitative trait, its genetic mechanism remains incomplete and requires further mining and dissection.

Given oligotrophic tolerance of tropical maize roots, genetic research remains lacking. Therefore, this study selected 241 maize inbred lines, conducted a pot experiment with karst soil, and systematically measured seven key root traits: root layer number, first-layer root number, second-layer root number, root angle, root area, maximum width, and total projected structure length. Combined with 64,666 high-quality SNP markers, GWAS was performed using the Bayesian-information and Linkage-disequilibrium Iteratively Nested Keyway (BLINK) model. On this basis, root transcriptome sequencing of deep-root inbred lines CIMBL111 and CML171 and the shallow-root inbred line IBC2 was further utilized to analyze expression differences of candidate genes among different genotypes, and qRT-PCR was used to validate key candidate genes. The results will provide a theoretical basis for genetic improvement of maize root architecture and gene resources for molecular breeding of nutrient-deficiency-tolerant and drought-resistant maize varieties in the karst mountainous region of Southwest China.

Materials and methods

Plant materials

A total of 241 maize inbred lines with wide genetic backgrounds were used in this study (Table S1; Luo et al. 2025). The experiment was conducted at the Teaching and Experiment Farm of Guizhou University (26°24'13.34" N, 106°40'19.51" E). This region has a subtropical monsoon humid climate, with an annual mean temperature of 14.9°C and annual mean rainfall of 1,200 mm. The 241 maize inbred lines were arranged in a completely randomized block design. Each material had two replicates and was sown on July 26, 2024, in plastic pots of 28 cm (width) × 25 cm (height). Three maize plants were grown in each replicate. The pots

were filled with a mixture of 30% humus substrate and 70% field soil. Appropriate amounts of urea and compound fertilizer were applied at the seedling stage. The field soil is classified as yellow soil (Haplic Alisol), which is a dominant soil type in the karst regions of southern China. Initial soil properties of the 0–20 cm soil layer were: pH of 5.15, electrical conductivity of 0.19 ms cm^{-1}, soil organic matter of 13.1 g kg^{-1}, total nitrogen of 1.28 g kg^{-1}, alkali hydrolyzable nitrogen of 27.8 mg kg^{-1}, available phosphorus of 15.1 mg kg^{-1}, and available potassium of 23.1 mg kg^{-1}. Roots were harvested at the late kernel dent stage, with six samples per material. After the maize roots were washed clean, three root trait data were collected manually. Subsequently, using a fixed camera position and a coin with a diameter of 2.5 cm as a reference, a total of 945 images were captured, numbered, and imported into the the Root Estimator for Shovelomics Traits (REST, version 1.0.1; Trachsel et al. 2011) software (Swiss Federal Institute of Agricultural Sciences, ETH Zurich) to obtain data for subsequent analyses.

Root trait measurement

This experiment mainly measured maize root layer number (RLN): the number of root layers was counted from the first aboveground root layer downward. First-layer root number (RN1stL): the number of maize roots produced from the first root layer, counted from the shoot–root junction downward. Second-layer root number (RN2ndL): the number of maize roots produced from the second root layer, counted from the shoot–root junction downward. Root area (Area): the area of all root pixels in the image, in cm^2. Root opening angle (RTO): the opening angle between the left and right root angles. Maximum width (MW): the maximum distance of the root system from left to right. Total projected structure length (TPSL): the projected distance from the shoot–root boundary as the starting point to the lowest root tip in the image. Root layer number and the numbers of first- and second-layer roots were collected manually, whereas root area, root angle, maximum width, and total projected structure length were collected by importing images of washed roots into the maize root analysis software REST 1.0.1. In this study, genotype was treated as a fixed factor and replication as a random factor. SAS 9.4 software (SAS Institute, Inc., Cary, NC, USA) was used for general linear model combined analysis of variance, correlation analysis, and best linear unbiased estimation (BLUE) of root-related data.

Genotypic data and genome-wide association analysis

The 241 maize inbred lines were genotyped by genotyping-by-sequencing using Illumina HiSeq 2000 at Beijing Compass Biotechnology Co., Ltd. After filtering for marker polymorphism, missing rate, and heterozygosity rate, 64,666 SNP markers were finally obtained. Details are described in Luo et al. (2025). Because these lines belong to the same population, the same genetic structure and linkage disequilibrium analysis results were used. In this study, LDKNNImputation in TASSEL 5.2.94 was used to impute missing genotypes, and SNPs that were heterozygous or missing among the 241 inbred lines were removed, retaining only homozygous markers.

In this study, the BLINK model in the GAPIT R package was used for GWAS analysis of the BLUE values of root phenotypes in the inbred association mapping population. Significant association signals were determined by quantile–quantile (QQ) plots; that is, the $-\log_{10}(p)$ value at which the observed $-\log_{10}(p)$ values clearly deviated from the expected $-\log_{10}(p)$ values under the null hypothesis was set as the threshold. In this study, $-\log_{10}(p) = 4$ was used as the significant association signal threshold. Based on the association mapping results and the linkage disequilibrium (LD) decay distance ($r^2 = 0.2$), genes within the 200 kb interval upstream and downstream of each significant SNP physical position were obtained as candidate genes based on the maize B73 reference genome (ZmB73_RefGen_v4; http://www.maizegdb.org/), and functional annotation was performed using MaizeGDB, NCBI, and online literature.

Transcriptome analysis

Based on the phenotypic identification results of the above association analysis, two deep-root inbred lines (CIMBL111 and CML171) and one shallow-root inbred line (IBC2) were selected for a pot experiment. At 30 days after sowing, three replicates at the V8 stage were selected for each inbred line, and all root tissues except brace roots were collected, immediately frozen in liquid nitrogen, and sent to Beijing Biomarker Technologies Co., Ltd. for library construction. DNase I was used to remove genomic DNA, and oligo(dT) magnetic beads were used to enrich mRNA, which was subsequently fragmented. The fragmented products were amplified by PCR, and samples were sequenced after passing in-house quality inspection. In data analysis, the maize genome ZmB73RefGen_v4 was used as the reference genome. Transcript or gene expression levels were expressed as fragments per kilobase of transcript per million mapped reads (FPKM). The threshold for significant differential gene expression was $p < 0.05$ and $|\log_2 FC| \geq 1$.

Identification and annotation of candidate genes

Gene Ontology (GO) enrichment analysis was used to identify all GO terms significantly enriched in differentially expressed genes (DEGs) relative to background genes. All DEGs were classified and grouped into GO terms using public databases. A hypergeometric test and Phytozome were used to identify significantly enriched GO terms. GO terms were divided into three categories: "biological process," "cellular component," and "molecular function." To further understand the biological functions of DEGs, enrichment analysis was performed using the KEGG pathway database. Genes were annotated using MaizeGDB and NCBI databases. Heatmaps were plotted using an online website.

Quantitative real-time PCR analysis

qRT-PCR was performed using the same total RNA as that used for transcriptome data analysis, isolated from roots of the deep-root inbred lines CIMBL111 and CML171 and the shallow-root inbred line IBC2 at the V8 stage. For each sample, cDNA was synthesized using the TransScript® One-Step gDNA Removal Kit and cDNA Synthesis SuperMix (TransGen Biotech, Beijing, China). qRT-PCR analysis was performed using a real-time PCR system (Analytik Jena, Germany). Actin was used as the internal control to normalize the obtained Ct values. Primer5.0 was used to design specific primers for this assay (Table S2). The 20 μl reaction mixture consisted of 2 μl cDNA, 7.2 μl ddH_2O, 0.4 μl each of forward and reverse primers (10 μM), and 10 μl 2× TransStart® Tip Green qPCR SuperMix (TransGen Biotech, Beijing, China). Relative gene expression was calculated using the $2^{-\Delta\Delta CT}$ method. Three biological replicates were combined for three technical replicates, and the average of the three replicates was used for gene expression analysis.

Results

Phenotypic description of seven root-related traits in the association population

In this study, seven root-related traits were measured across 241 maize inbred lines (Fig. 1; Table S3), which exhibited abundant phenotypic variation in roots. RLN varied from 3.98 to 7.00 layers, averaging 5.43 layers; the highest RLN was observed in 04K5672 (7.00), L135, IRF291, CML171, and CIMBL111, whereas the lowest was recorded in By807 (3.98), GEMS28, DH3732, Mo17, CF3, and Dong46. RN1stL showed a range of 3.97–19.37, with a mean of 11.23; L135 and Yu374 had the highest values, while Zi330 had the lowest. For RN2ndL, values spanned 3.86–15.16 (mean = 9.00), with L135 and PhT10 displaying the maximum and minimum, respectively. RTO ranged from 9.96° to 119.35°, averaging 40.02°; Zheng30, CIMBL111, and GEMS31 exhibited the largest angles, whereas WH413, 384-2, and IBC2 had the smallest. Area varied between 3.46 and 113.82 cm^2 (mean = 37.60 cm^2), with Dan340, CML171, and Zheng30 showing the highest values and PB807, PB80, and 1108-3 the lowest. MW ranged from 3.18 to 12.14 cm, averaging 6.92 cm; the maximum MW occurred in CIMBL111, CIMBL14, and Dan340, and the minimum in PB80, LH149, and 17Dong64. TPSL spanned 39.4–1,846.11 (mean = 613.80), with Dan340, CML171, and GEMS31 having the highest values and By807, PB80, and LH149 the lowest. The coefficients of variation for all seven traits exceeded 10%, with RTO (32.96%), Area (49.50%), and TPSL (48.73%) showing particularly large variation ranges. Based on skewness and kurtosis together with histogram distributions (Fig. 1), the absolute values for most traits were below 1, consistent with the typical characteristics of polygenic quantitative traits. ANOVA revealed significant differences among inbred lines for all seven root-related traits (Table S4), indicating genetic control. Correlation analysis further showed trait correlations to varying degrees, reflecting synergistic and differentiated features among root architecture components (Fig. 2). Specifically, Area was positively and significantly correlated with RTO, MW, and TPSL at medium to high levels (r = 0.90, 0.72, and 0.61, respectively), suggesting that root surface area is mainly determined by horizontal extension and maximum width; MW was significantly positively correlated with RTO (r = 0.74), indicating that maximum root width also influences root angle; TPSL was moderately positively correlated with RTO and MW (r = 0.50 and 0.61). In addition, RN1stL was significantly positively correlated with RN2ndL (r = 0.76).

Genome-wide association analysis

To identify genetic loci affecting maize roots, we used 64,666 SNPs in an association population of 241 maize inbred lines to conduct a comprehensive GWAS for seven root-related traits. The significance threshold was set at $-\log_{10}(p) = 4.0$ for six traits and $-\log_{10}(p) = 3.5$ for root area, and the BLINK method was used. A total of 24 QTL containing 73 significant SNPs were detected (Table 1; Fig. 3). The fewest QTL were observed for MW and TPSL (one each), and the most were nine QTL associated with RN2ndL. These QTL were distributed on seven chromosomes except chromosomes 2, 4, and 10, with an average of 14.8 significant SNPs per chromosome, ranging from one on chromosome 1 to five on chromosomes 5 and 9 (Table 1). A total of 66.7% of the detected loci explained less than 5% of phenotypic variation (PVE), indicating that root architecture is mainly controlled by minor-effect loci.

Root layer number

A total of two significant SNPs were detected for RLN on chromosomes 1 and 6. The most significant SNP, Chr6_144810245, was located on chromosome 6, with a p value of 5.83×10^{-5}, MAF of 0.41, additive effect of 0.18, and allele A/C frequency ratio of 171/64; it explained 7.94% of phenotypic variation. Another significant SNP, Chr1_264008402, was located on chromosome 1, with a p value of 7.20×10^{-5}, MAF of 0.27, additive effect of 0.18, and allele T/G frequency ratio of 138/97; it explained 7.45% of phenotypic variation.

First-layer root number

A total of four QTL (38 significant SNPs) associated with RN1stL were detected on chromosomes 6, 7, and 8. Among them, two QTL (36 significant SNPs) were detected on chromosome 7, namely Chr7_92154793 and Chr7_92897447, with p values of 6.17×10^{-5} and 6.01×10^{-5}, MAF of 0.22 and 0.23, and additive effects of 0.78 and 0.77, respectively. One significant SNP, Chr8_172156463, was detected on chromosome 8, with a p value of 6.10×10^{-5}, MAF of 0.22, additive effect of 0.83, allele G/A frequency ratio of 184/51, and PVE of 5.61%. One significant SNP, Chr6_143935680, was also detected on chromosome 6, with a p value of

7.91×10^{-5}, MAF of 0.22, additive effect of −1.33, allele A/G frequency ratio of 222/13, and PVE of 11.39%, making it the locus with the highest PVE detected for RN1stL.

Second-layer root number

A total of nine QTL (23 significant SNPs) associated with RN2ndL were detected, the most among all traits, distributed on chromosomes 3, 5, 7, and 8. Two QTL (three significant SNPs) were detected on chromosome 3, with additive effects of −0.99 and −1.12, respectively; among them, Chr3_199104155 had a PVE of 13.40%, the highest for this trait. Four QTL (six significant SNPs) were detected on chromosome 5, among which Chr5_72720076 had a p value of 2.65×10^{-5}, allele A/G frequency ratio of 167/68, and PVE of 4.31%, the highest on chromosome 5. Two significant SNPs were detected on chromosome 7, among which Chr7_113941163 had a PVE of 1.51%. One QTL (12 significant SNPs) was detected on chromosome 8, representing the densest signal region for this trait. The most significant SNP in this interval, Chr8_141040704, had a p value of 1.25×10^{-5}, MAF of 0.26, additive effect of −0.71, and PVE of 2.85%.

Root angle

A total of two significantly associated SNPs, Chr6_154179827 and Chr9_131195413, were detected for RTO on chromosomes 6 and 9. The most significant SNP, Chr9_131195413, had MAF of 0.08, additive effect of −7.32, allele A/C frequency ratio of 147/71, and PVE of 1.00%.

Root area

At the significance threshold of 1×10^{-4}, no significant SNP was detected for Area. When the threshold was lowered to $1 \times 10^{-3.5}$, a total of five QTL (six significant SNPs) associated with Area were detected on chromosomes 3, 5, 8, and 9. One QTL (two significant SNPs) was detected on chromosome 3, among which Chr3_198630019 had a p value of 1.54×10^{-4}, MAF of 0.20, additive effect of −6.66, and PVE of 1.80%. One significant SNP, Chr5_76825409, was detected on chromosome 5, with a p value of 2.91×10^{-4}, MAF of 0.41, additive effect of 5.16, and PVE of 2.52%, the highest for this trait. One significant SNP, Chr8_93642581, was detected on chromosome 8, with a p value of 3.13×10^{-4}, MAF of 0.12, additive effect of −7.91, and PVE of 0.12%. Two significant SNPs were detected on chromosome 9, with p values of 2.68×10^{-4} and 2.29×10^{-4}; both had negative additive effects.

Maximum width and total projected structure length

At the threshold of 1×10^{-4}, one significant SNP was detected for each of MW and TPSL, both located on chromosome 9. The significant SNP for MW was Chr9_40082086, with a p value of 2.76×10^{-5}, MAF of 0.05, additive effect of −1.12, and PVE close to zero. The significant SNP for TPSL was Chr9_65977657, with a p value of 5.71×10^{-5}, MAF of 0.05, additive effect of −1.12, allele G/A frequency ratio of 160/68, and PVE of 14.43%, the highest among all loci detected in this GWAS.

Candidate genes and functional annotation

In this study, a total of 24 QTL (73 significant SNP loci; Table 1 and Table S5) associated with maize root-related traits were screened. To further explore candidate genes affecting maize root-related traits, candidate genes were screened and annotated within ±200 kb of these significant loci using MaizeGDB and NCBI databases. Finally, 29, 55, 109, 22, 59, 3, and 3 candidate genes were identified for RLN, RN1stL, RN2ndL, RTO, Area, MW, and TPSL, respectively (Table S5). Functional annotation classified these candidate genes into transcription factors (including MYB, AP2/EREBP, bZIP, NAC, TCP, GRF, Dof, G2-like, GNAT, CO-like, PHD, and other families), protein kinases (such as serine/threonine protein kinases, receptor-like protein kinases, and CK2 protein kinases), molecular chaperones/heat shock proteins (such as HSP20 and DnaJ), hormone metabolism- and signaling-related genes (such as gibberellin 2-oxidase and jasmonate-regulated genes), cell wall-modifying enzymes (such as pectinesterase, polygalacturonase, and endoglucanase), and many other structural proteins and uncharacterized proteins with catalytic, transport, or binding functions. GO enrichment analysis (Fig. S1) showed significant enrichment in ubiquitin–proteasome-dependent protein catabolic process, protein glycosylation, and glycoprotein biosynthetic process, as well as in the SCF/cullin-RING ubiquitin ligase complex, suggesting that protein degradation and glycosylation may participate in the regulation of root architecture; in terms of molecular function, ubiquitin transferase activity, nuclease activity, and oxidoreductase activity were enriched.

Transcriptome analysis

In this study, deep-root maize inbred lines CIMBL111 and CML171 and the shallow-root inbred line IBC2 were selected, and genome-wide gene expression levels in V8-stage roots were analyzed by RNA-seq. Based on the Illumina high-throughput sequencing platform, nine maize samples (three genotypes CIMBL111, CML171, and IBC2, each with three biological replicates) were subjected to eukaryotic reference transcriptome sequencing, yielding a total of 55.46 Gb of clean data. Clean data for each sample reached more than 5.74 Gb, and the percentage of bases with quality score Q30 was not less than 97.75%, indicating sufficient and high-quality sequencing output. After aligning clean reads to the specified reference genome (Zea_mays Zm_B73_REFERENCE_4.0), the alignment efficiency of each sample was 85.09%–90.20%, among which the proportion of unique mapped reads ranged from 82.25% to 87.21%, indicating that the selected reference genome could well meet the analytical requirements of this study. The results showed that the mature root structure of CML171 and CIMBL111 was deep-rooted, whereas IBC2 was shallow-rooted

(Fig. 4A); RLN, RN2ndL, Area, MW, and TPSL of CML171 and CIMBL111 were significantly higher than those of IBC2 (Fig. 4B). In this study, the threshold for significant differential expression of root genes was set at $p < 0.05$ and $|\log_2 FC| \geq 1$. Therefore, in the IBC2_vs_CIMBL111 group, there were 8,032 DEGs, including 2,863 up-regulated and 5,169 down-regulated genes. In the IBC2_vs_CML171 group, there were 9,299 DEGs, including 3,617 up-regulated and 5,682 down-regulated genes (Fig. 4C). Notably, the numbers of genes commonly up-regulated and down-regulated in the two groups were 944 and 3,553, respectively. On this basis, GO enrichment analysis (including the three branches BP, CC, and MF) and KEGG pathway classification and enrichment analysis were performed for the differential gene sets. GO enrichment analysis of candidate genes showed that biological process involved cellular and metabolic process and biological regulation; cellular component involved cellular anatomical entity, intracellular, and protein-containing complex; and molecular function mainly involved catalytic activity, binding, and transporter activity (Fig. 4D). KEGG enrichment analysis of the two transcriptome groups showed that the genes were related to phenylpropanoid biosynthesis, starch and sucrose metabolism, glutathione metabolism, and benzoxazinoid biosynthesis (Fig. 4E). In summary, the sequencing data in this study had high quality, and the bioinformatics analysis pipeline was systematic and comprehensive. The obtained new genes, lists of differentially expressed genes, and functional enrichment results provide a detailed and reliable data foundation for further exploration of the molecular regulatory mechanisms underlying differences in root architecture traits among different maize varieties.

Candidate genes obtained by integrating transcriptome analysis and GWAS

In this study, 280 candidate genes were obtained by GWAS and 12,342 DEGs were obtained by RNA-seq; subsequently, by integrating GWAS and RNA-seq analysis, 62 candidate genes related to root architecture were jointly identified (Fig. 5A). The above 62 candidate genes exhibited eight expression patterns in the V8-stage shallow-root and deep-root transcriptomes (Fig. 5B): nine candidate genes were commonly down-regulated in both IBC2_vs_CIMBL111 and IBC2_vs_CML171; three candidate genes were commonly up-regulated in both IBC2_vs_CIMBL111 and IBC2_vs_CML171; two candidate genes were down-regulated in IBC2_vs_CIMBL111 but up-regulated in IBC2_vs_CML171; one candidate gene was up-regulated in IBC2_vs_CIMBL111 but down-regulated in IBC2_vs_CML171; 14 and 11 candidate genes were only down-regulated and up-regulated, respectively, in IBC2_vs_CML171; and nine and 13 candidate genes were only down-regulated and up-regulated, respectively, in IBC2_vs_CIMBL111. Subsequently, based on the three main-effect QTL in the GWAS results (Table 1), the SNP Chr6_143935680 most significantly associated with RN1stL (Fig. 5C) and the SNP Chr9_65977657 most significantly associated with Area and TPSL (Fig. 5D) were selected. Meanwhile, the haplotype A/G of Chr6_143935680 simultaneously affected RN1stL and RN2ndL (Fig. 5E), and the haplotype G/A of Chr9_65977657 simultaneously affected MW, RTO, Area, and TPSL (Fig. 5F). From the 12 commonly up-regulated or commonly down-regulated candidate genes, Zm00001d014443 and Zm00001d046300 were selected for qPCR validation, and the results showed that their trends were consistent with the transcriptome data (Fig. 5G). Within the QTL confidence interval of SNP Chr6_143935680, there were 16 candidate genes, among which only Zm00001d037968 and Zm00001d037969 were detected among the transcriptome differentially expressed candidate genes; qPCR results further showed that both were extremely significantly down-regulated in IBC2_vs_CML171 (Fig. 5H), whereas Zm00001d037969 was significantly up-regulated in IBC2_vs_CIMBL111. Zm00001d037968 encodes a PAR1 protein, and Zm00001d037969 encodes an Inhibitor I family protein. Within the QTL confidence interval of SNP Chr9_65977657, there were three candidate genes, among which only the differentially expressed gene closest to the most significant SNP, Zm00001d046136, was validated by qPCR to be significantly down-regulated in IBC2_vs_CIMBL111 (Fig. 5H; Fig. 5E). Zm00001d046136 encodes a GDSL esterase/lipase. In summary, through comprehensive analysis of GWAS and RNA-seq data, this study identified 62 differential candidate genes and, combined with two main-effect loci, screened three candidate genes, providing new gene resources for future breeding of deep-root maize inbred lines.

Discussion

Significant differences in maize root traits among diverse genetic backgrounds

Roots are important organs for water and nutrient uptake in maize, so dissecting genetics of root architecture is of great significance. In this study, seven root-related traits of 241 maize inbred lines mostly showed typical quantitative trait characteristics, conforming to normal distributions and exhibiting rich phenotypic variation, consistent with the results of (Li et al. 2020, 2023, 2024, 2025). Maize is a typical fibrous-root crop; after field planting, sampling easily causes root loss, and sampling is difficult and labor-intensive. Therefore, most early root genetic studies were conducted at the seedling stage or in laboratory experiments such as hydroponics (Hochholdinger 2009; Lebreton et al. 1995; Pace et al. 2015; Salvi et al. 2016; Song et al. 2016; Zhang et al. 2026). At present, most genetic reports based on field sampling have been conducted in regions with better soil conditions (Cai et al. 2012; Li et al. 2020, 2023, 2024; Ren et al. 2022; Wu et al. 2022), whereas studies in Southwest China, where soil is compacted, clayey, shallow, and poor, are relatively scarce. In this study, a mixture of 30% humus substrate and 70% typical zonal yellow soil from Guizhou was used, and large-pot cultivation combined with open-air cultivation was adopted to identify mature-stage root traits of 241 maize

materials, which not only reduced root sampling loss but also took into account native soil conditions and the field environment. This study found that inbred lines from temperate germplasm had significantly fewer RN2ndL and narrower MW than those from tropical germplasm (Fig. S2), consistent with the report of Wu et al. (2022) that the SS subgroup had steeper and narrower root systems than other subgroups. Therefore, tropical maize materials have more vigorous root systems and should be used more in subsequent breeding research. In addition, based on comprehensive analysis of all root traits using the membership function method, and comparing the root phenotypic data of Ren et al. (2022), Wu et al. (2022), and this study (results not shown), we found that the core germplasm Dan340 and Zheng30, which had coordinated excellent performance in multiple root traits and ranked in the top 10% comprehensively in this study, also performed well in Ren et al. (2022); the deep-root inbred lines Zheng32, TY4, CIMBL14, R08, and CML171 were also located in the top 20% of excellent materials in Wu et al. (2022), showing large root area, wide roots, and deep roots. Among them, TY4, CIMBL14, and CML171 are derived from tropical germplasm, and Zheng32 and R08 are derived from mixed temperate and tropical germplasm. On the other hand, the shallow-root inbred lines Wu109, WH413, By807, and Shen135 identified in this study were also consistent with the reports of Wu et al. (2022) and Ren et al. (2022), respectively. Cross-validation among the above studies further confirmed the deep-root and oligotrophic tolerance characteristics of tropical maize germplasm, and the tropical inbred line CML171 can serve as an excellent donor parent for genetic improvement of maize roots. The screening of the above extreme materials provides core parent resources for the subsequent construction of genetic populations and mining of key genes regulating root traits.

Co-localization with known QTL and discovery of novel loci reveal complex genetic regulation of maize root architecture

Up to now, lots of studies have used linkage aand association analysis to map genetic loci regulating root architecture traits (Cai et al. 2012; Hochholdinger 2009; Lebreton et al. 1995; Li et al. 2023; Li et al. 2020; Li et al. 2024; Pace et al. 2015; Ren et al. 2022; Salvi et al. 2016; Song et al. 2016; Wu et al. 2022; Zhang et al. 2026), providing important references for further dissection of the genetic basis of maize root architecture in this study. In this study, GWAS was performed for seven maize root traits, and a total of 24 related QTL (composed of 73 significant SNPs) were detected, among which multiple loci were consistent with previous studies (Li et al. 2024; Ren et al. 2022). Specifically, Chr1_264008402 associated with RLN and the genetic loci controlling the number of shoot-borne brace root whorls (ANN) and shoot-borne brace root number above aboveground whorl 2 (AW2) reported by Li et al. (2024) were all located in the 163.1–164.9 Mb interval on chromosome 1. Similarly, Chr3_199104155 affecting RN2ndL and the AW2-associated locus chr3.5_199250880 reported by Li et al. (2024) were located in the adjacent interval. In addition, Chr6_144810245 significantly affected RLN in this study, whereas it was found to be significantly associated with total shoot-borne root number (ARN) in Li et al. (2024); meanwhile, qARN26-1 associated with axial root number mapped by Cai et al. (2012) was also located in the same Bin 6.05. Similarly, Chr7_2679841 and Chr8_141040704 associated with RN2ndL co-localized with loci significantly associated with AW2 and ANN, respectively, in Li et al. (2024). In addition, Chr6_154179827 controlling RTO was adjacent to the locus chr6.5_154160512 controlling top root angle in Ren et al. (2022); in this Bin 6.06, Li et al. (2020) also detected a QTL related to crown root angle (CRA). Notably, Chr7_92154793 affecting RN1stL in this study was located in a region similar to PZE-107045046 associated with total number of root whorls (TNN) reported by Li et al. (2024). In the 46–76 Mb interval of chromosome 5, we detected five QTL associated with RN2ndL and Area. Zhang et al. (2023) identified a major QTL, qLRT5-1, controlling lateral root number at 87 Mb on the same chromosome and confirmed that its candidate gene participates in lateral root development regulation. The QTL detected in this study and qLRT5-1 are located on the same chromosome, indicating that there may be multiple independent functional loci regulating different types of root number on chromosome 5, jointly participating in the genetic regulation of maize root number traits. The above co-localization results support the reliability of the results of this study; at the same time, the current study also discovered some novel loci and reveal complex genetic regulation of maize root architecture, laying a foundation for subsequent research to dissect new genetic mechanisms of maize roots.

Joint analysis suggests candidate genes potentially involved in genetic regulation of maize root architecture

In this study, 24 QTL were detected by GWAS, and a total of 280 candidate genes were identified within ±200 kb of the significant loci. Combined with DEGs from RNA-seq of deep-root and shallow-root inbred lines, 62 candidate genes were obtained by joint analysis, and their functional annotations involve multiple biological processes such as transcriptional regulation, signal transduction, and hormone metabolism. These genes provide important clues for understanding the molecular regulatory mechanisms of maize root structure. Within 10 Mb flanking regions of the significantly associated loci, we found five genes with reported functions in root development. Specifically, *ZmCIPK15* and *TB1* are located near Chr1_264008402 associated with RLN, among which *ZmCIPK15* regulates maize root angle (Schneider et al. 2022) and *TB1* affects modern maize roots (Gaudin et al. 2014); *RTH5*, which affects root hair elongation (Nestler et al. 2014), is located near Chr3_185631059 associated with RN2ndL; *ARGOS8*, which affects nodal root number (Shi et al. 2015), is located near Chr6_144810245 associated with RLN; and *RAP2.7*, which participates in

maize brace root development (Li et al. 2019), is located near Chr8_141040704 associated with RN2ndL. The proximity of the above known genes to the associated loci provides direct clues for candidate gene screening at the corresponding loci. In addition to known genes near the loci, some of the 61 candidate genes have also been functionally reported. Notably, Jiang et al. (2021) reported that the triple mutant of *ZmTGA9-3* (Zm00001d012294) and two homologous genes showed complete male sterility, whereas double or single mutants were male fertile; this gene is currently mainly associated with reproductive development, and whether it participates in root architecture regulation needs further validation. Liu et al. (2023) identified the metal transporter *ZmNRAMP6* (Zm00001d015133) through genome-wide trait-associated co-expression network analysis; *ZmNRAMP6* confers Pb sensitivity by accumulating Pb to maize shoots, and its mutant shows greater total root length than the wild type under normal conditions, suggesting that this gene may affect root growth through metal stress response pathways. Wang et al. (2021) map-based cloned the teosinte-derived *ZmMM1* (Zm00001d018698) resistance allele, revealing that a 3'UTR variant increases protein accumulation and that it acts as a transcriptional repressor negatively regulating target genes such as *ZmMT3*, thereby conferring resistance to NLB, GLS, and SCR. The above genes are involved in root development, metal stress response, and disease resistance, providing references for subsequent functional validation of candidate genes and genetic dissection of root architecture. For the three key candidate genes Zm00001d037968, Zm00001d037969, and Zm00001d046136, limited information is available regarding their functions. Therefore, further functional validation using mutant and overexpression lines is warranted in the future.

Acknowledgements

This work was financed and supported by the National Natural Science Foundation of China (32501908), Guizhou Provincial Basic Research Program (Natural Science, Qiankehe Jichu ZD[2026]024), Emerging Talent Team for Maize Bio-breeding with Stress Resistance, High Efficiency, and High Yield (Qian Nong Ke Yuan Emerging Talent Team Grant No. [2026] 02), Guizhou Key Laboratory of High Quality, High Efficiency, and Yield Enhancement in Grain and Oil Crops (Qian-Ke-He-Platform ZSYS[2025]037), Basic Research Projects of Guizhou University[grant No.(2023) 37].

Contributions

QY, HDM, and XBH conceived and designed the experiments. MYZ, MY, YJL, JYX, and YFL performed the experiments, with assistance from ZHP, YLJ, XW, and QY. MYZ, MY, and YJL analyzed the data under the guidance of YC. YX assisted with soil composition measurements. ZMY wrote the manuscript, and QY, HDM, and XBH revised it. QY, HDM, and XBH submitted the final version. All authors read and approved the final manuscript.

Ethics declarations

Conflict of interest

The authors have no relevant financial or nonfinancial interests to disclose.

References:

Bray AL, Topp CN (2018) The quantitative genetic control of root architecture in maize. Plant and Cell Physiology 59: 1919–1930. https://doi.org/10.1093/pcp/pcy141.

Cai H, Chen F, Mi G, Zhang F, Maurer HP, Liu W, Reif JC, Yuan L (2012) Mapping QTLs for root system architecture of maize (*Zea mays* L.) in the field at different developmental stages. Theoretical and Applied Genetics 125: 1313–1324. https://doi.org/10.1007/s00122-012-1915-6.

Chen Z (2024) Cultivated land quality assessment, obstacle factors, and yield improvement potential in the Yunnan–Guizhou Plateau. Master's/Doctoral dissertation, Yunnan Agricultural University.

Emerson RA, Beadle GW, AC F (1935) A summary of linkage studies in maize. Cornell University Agricultural Experiment Station Memoir, 180: 40–42.

Fang S, Ji M, Zhu T, Wang Y, Tang X, Zhu X, Yang Z, Xu C, Wang H, Li P (2024) Multi-omics analysis reveals the transcriptional regulatory network of maize roots in response to nitrogen availability. Agronomy 14: 1541. https://www.mdpi.com/2073-4395/14/7/1541.

Gaudin ACM, McClymont SA, Soliman SSM, Raizada MN (2014) The effect of altered dosage of a mutant allele of *Teosinte branched 1* (*tb1-ref*) on the root system of modern maize. BMC Genetics 15: 23. https://doi.org/10.1186/1471-2156-15-23.

Guo W, Wang F, Lv J, Yu J, Wu Y, Wuriyanghan H, Le L, Pu L (2025) Phenotyping, genome-wide dissection, and prediction of maize root architecture for temperate adaptability. iMeta 4: e70015. https://doi.org/10.1002/imt2.70015.

He K, Zhao Z, Ren W, Chen Z, Chen L, Chen F, Mi G, Pan Q, Yuan L (2023) Mining genes regulating root system architecture in maize based on data integration analysis. Theoretical and Applied Genetics 136: 127. https://doi.org/10.1007/s00122-023-04376-0.

Hetz W, Hochholdinger F, Schwall M, Feix G (1996) Isolation and characterization of *rtcs*, a maize mutant deficient in the formation of nodal roots. The Plant Journal 10: 845–857. https://doi.org/10.1046/j.1365-313X.1996.10050845.x.

Hochholdinger F (2009) The maize root system: morphology, anatomy, and genetics. In: JL Bennetzen, SC Hake (eds) Handbook of maize: its biology. Springer New York, NY.

Hochholdinger F, Feix G (1998) Early post-embryonic root formation is specifically affected in the maize mutant *lrt1*. The Plant Journal 16: 247–255. https://doi.org/10.1046/j.1365-313x.1998.00280.x.

Hochholdinger F, Park WJ, Feix GnH (2001) Cooperative Action of *SLR1* and *SLR2* Is Required for Lateral Root-Specific Cell Elongation in Maize. Plant Physiology 125: 1529–1539. https://doi.org/10.1104/pp.125.3.1529.

IPCC, 2019: Climate Change and Land: an IPCC special report on climate change, desertification, land degradation, sustainable land management, food security, and greenhouse gas fluxes in terrestrial ecosystems [P.R. Shukla, J. Skea, E. Calvo Buendia, V. Masson-Delmotte, H.-O. Pörtner, D. C. Roberts, P. Zhai, R. Slade, S. Connors, R. van Diemen, M. Ferrat, E. Haughey, S. Luz, S. Neogi, M. Pathak, J. Petzold, J. Portugal Pereira, P. Vyas, E. Huntley, K. Kissick, M. Belkacemi, J. Malley, (eds.)]. In press.

Jiang Y, An X, Li Z, Yan T, Zhu T, Xie K, Liu S, Hou Q, Zhao L, Wu S, Liu X, Zhang S, He W, Li F, Li J, Wan X (2021) CRISPR/Cas9-based discovery of maize transcription factors regulating male sterility and their functional conservation in plants. Plant Biotechnology Journal 19: 1769–1784. https://doi.org/10.1111/pbi.13590.

Jing J, Gao W, Cheng L, Wang X, Duan F, Yuan L, Rengel Z, Zhang F, Li H, Cahill JF, Shen J (2022) Harnessing root-foraging capacity to improve nutrient-use efficiency for sustainable maize production. Field Crops Research 279: 108462. https://doi.org/10.1016/j.fcr.2022.108462.

Lebreton C, Lazić-Jančić V, Steed A, Pekić S, Quarrie SA (1995) Identification of QTL for drought responses in maize and their use in testing causal relationships between traits. Journal of Experimental Botany 46: 853–865. https://link.cnki.net/doi/10.27458/d.cnki.gynyu.2024.000967.

Li C, Guo J, Wang D, Chen X, Guan H, Li Y, Zhang D, Liu X, He G, Wang T, Li Y (2023) Genomic insight into changes of root architecture under drought stress in maize. Plant, Cell and Environment 46: 1860–1872. https://doi.org/10.1111/pce.14567.

Li J, Chen F, Li Y, Li P, Wang Y, Mi G, Yuan L (2019) *ZmRAP2.7*, an AP2 transcription factor, is involved in maize brace roots development. Frontiers in Plant Science 10: 820. https://www.frontiersin.org/journals/plant-science/articles/10.3389/fpls.2019.00820.

Li P, Fan Y, Yin S, Wang Y, Wang H, Xu Y, Yang Z, Xu C (2020) Multi-environment QTL mapping of crown root traits in a maize RIL population. The Crop Journal 8: 645–654. https://doi.org/10.1016/j.cj.2019.12.006.

Li P, Zhang Z, Xiao G, Zhao Z, He K, Yang X, Pan Q, Mi G, Jia Z, Yan J, Chen F, Yuan L (2024) Genomic basis determining root system architecture in maize. Theoretical and Applied Genetics 137: 102. https://doi.org/10.1007/s00122-024-04606-z.

Li P, Zhu T, Wang Y, Zhang X, Yang X, Fang S, Li W, Rui W, Yang A, Duan Y, Yan Y, Pan Q, Jia Z, Wang H, Yang Z, Yu P, Xu C (2025) Natural variation in a cortex/epidermis-specific transcription factor *bZIP89* determines lateral root development and drought resilience in maize. Science Advances 11: eadt1113. https://doi.org/10.1126/sciadv.adt1113.

Liu P, Jiang L, Long P, Li Q, Hou F, Yuan G, Chen Z, Zhang M, Zou C, Pan G, Ma L, Shen Y (2023) A genome-wide co-expression network analysis revealed *ZmNRAMP6*-mediated regulatory pathway involved in maize tolerance to lead stress. Theoretical and Applied Genetics 136: 122. https://doi.org/10.1007/s00122-023-04371-5.

Luo J, Li Y, Jiang Y, Zhang X, Bai G, Peng Z, Yi Q, Hou X (2025) Integrative mapping in large inbred and hybrid association panels along with an F_2 population advanced a novel understanding of general combining ability for plant height in maize. Theoretical and Applied Genetics, 138(4), 1–15. https://doi.org/10.1007/s00122-025-04883-2.

Nestler J, Liu S, Wen T-J, Paschold A, Marcon C, Tang HM, Li D, Li L, Meeley RB, Sakai H, Bruce W, Schnable PS, Hochholdinger F (2014) *Roothairless5*, which functions in maize (*Zea mays* L.) root hair initiation and elongation encodes a monocot-specific NADPH oxidase. The Plant Journal 79: 729–740. https://doi.org/10.1111/tpj.12578.

Pace J, Gardner C, Romay C, Ganapathysubramanian B, Lübberstedt T (2015) Genome-wide association analysis of seedling root development in maize (*Zea mays* L.). BMC Genomics 16: 47. https://doi.org/10.1186/s12864-015-1226-9.

Ren W, Zhao L, Liang J, Wang L, Chen L, Li P, Liu Z, Li X, Zhang Z, Li J, He K, Zhao Z, Ali F, Mi G, Yan J, Zhang F, Chen F, Yuan L, Pan Q (2022) Genome-wide dissection of changes in maize root system architecture during modern breeding. Nature Plants 8: 1408–1422. https://doi.org/10.1016/j.fcr.2022.108462.

Salvi S, Giuliani S, Ricciolini C, Carraro N, Maccaferri M, Presterl T, Ouzunova M, Tuberosa R (2016) Two major quantitative trait loci controlling the number of seminal roots in maize co-map with the root developmental genes *rtcs* and *rum1*. Journal of Experimental Botany 67: 1149–1159. https://doi.org/10.1016/j.fcr.2022.108462.

Schneider HM, Lor VS, Zhang X, Saengwilai P, Hanlon MT, Klein SP, Davis JL, Borkar AN, Depew CL, Bennett MJ, Kaeppler SM, Brown KM, Bhosale R, Lynch JP (2023) Transcription factor *bHLH121* regulates root cortical aerenchyma formation in maize. Proceedings of the National Academy of Sciences 120: e2219668120. https://doi.org/10.1073/pnas.2219668120.

Schneider HM, Lor VSN, Hanlon MT, Perkins A, Kaeppler SM, Borkar AN, Bhosale R, Zhang X, Rodriguez J, Bucksch A, Bennett MJ, Brown KM, Lynch JP (2022) Root angle in maize influences nitrogen capture and is regulated by calcineurin B-like protein (CBL)-interacting serine/threonine-protein kinase 15 (*ZmCIPK15*). Plant Cell Environment 45: 837–853. https://doi.org/10.1111/pce.14135.

Shi J, Habben JE, Archibald RL, Drummond BJ, Chamberlin MA, Williams RW, Lafitte HR, Weers BP (2015) Overexpression of *ARGOS* genes modifies plant sensitivity to ethylene, leading to improved drought tolerance in both *arabidopsis* and Maize. Plant Physiology 169: 266–282. https://doi.org/10.1104/pp.15.00780.

Song W, Wang B, Hauck AL, Dong X, Li J, Lai J (2016) Genetic dissection of maize seedling root system architecture traits using an ultra-high density bin-map and a recombinant inbred line population. Journal of Integrative Plant Biology 58: 266–279. https://doi.org/10.1111/jipb.12452.

Stamp P, Kiel C (1992) Root morphology of maize and its relationship to root lodging. Journal of Agronomy and Crop Science 168: 113–118. https://doi.org/10.1111/j.1439-037X.1992.tb00987.x.

Taramino G, Sauer M, Stauffer JL, Jr., Multani D, Niu X, Sakai H, Hochholdinger F (2007) The maize (*Zea mays* L.) *RTCS* gene encodes a LOB domain protein that is a key regulator of embryonic seminal and post-embryonic shoot-borne root initiation. The Plant Journal 50: 649–659. https://doi.org/10.1111/j.1365-313X.2007.03075.x.

Wang H, Hou J, Ye P, Hu L, Huang J, Dai Z, Zhang B, Dai S, Que J, Min H, Chen G, Wang Y, Jiang M, Liang Y, Li L, Zhang X, Lai Z (2021) A teosinte-derived allele of a MYB transcription repressor confers multiple disease resistance in maize. Molecular Plant 14: 1846–1863. https://doi.org/10.1016/j.molp.2021.07.008.

Wang T, Wang F, Deng S, Wang K, Feng D, Xu F, Guo W, Yu J, Wu Y, Wuriyanghan H, Li S-T, Gu X, Le L, Pu L (2025) Single-cell transcriptomes reveal spatiotemporal heat stress response in maize roots. Nature Communications 16: 177. https://doi.org/10.1038/s41467-024-55485-3.

Wei Q, Yang Q, Wang W, XU LJ (2026) Effects of terrain–climate interactions on regional precipitation distribution in mountainous areas of Guizhou. Meteorological,Hydrological and Marine Instruments 43: 82–85+90. https://link.cnki.net/doi/10.19441/j.cnki.issn1006-009x.2026.03.026.

Wen T-J, Schnable PS (1994) Analyses of mutants of three genes that influence root hair development in *Zea mays* (Gramineae) suggest that root hairs are dispensable. American Journal of Botany 81: 833–842. https://doi.org/10.1002/j.1537-2197.1994.tb15564.x.

Woll K, Borsuk L, Stransky H, Nettleton D, Schnable PS, Hochholdinger F (2005) Isolation, characterization and pericycle specific transcriptome analyses of the novel maize (*Zea mays* L.) lateral and seminal root initiation mutant *rum1*. Plant Physiology 139: 1255–1267.

Wu B, Ren W, Zhao L, Li Q, Sun J, Chen F, Pan Q (2022) Genome-Wide Association Study of Root System Architecture in Maize. Genes (basel) 13(2):181

Zhan A, Schneider H, Lynch JP (2015) Reduced lateral root branching density improves drought tolerance in maize. Plant Physiology 168: 1603–1615. https://doi.org/10.1104/pp.15.00187.

Zhang M, Chen Y, Xing H, Ke W, Shi Y, Sui Z, Xu R, Gao L, Guo G, Li J, Xing J, Zhang Y (2023) Positional cloning and characterization reveal the role of a miRNA precursor gene *ZmLRT* in the regulation of lateral root number and drought tolerance in maize. Journal of Integrative Plant Biology 65: 772–790. https://doi.org/10.1111/jipb.13408.

Zhang X, Wang H, Shen M, Zhu Y, Cheng H, Chen R, Yang X, Li Y, Li D, Nie M, Fang H, Li Z, Zhang M, Zhu Y, Hu Z, Li P (2026) Natural variation in *ZmHSP20-5* enhances root growth and drought tolerance in maize. The Crop Journal 14: 517–528. https://doi.org/10.1016/j.cj.2025.11.021.

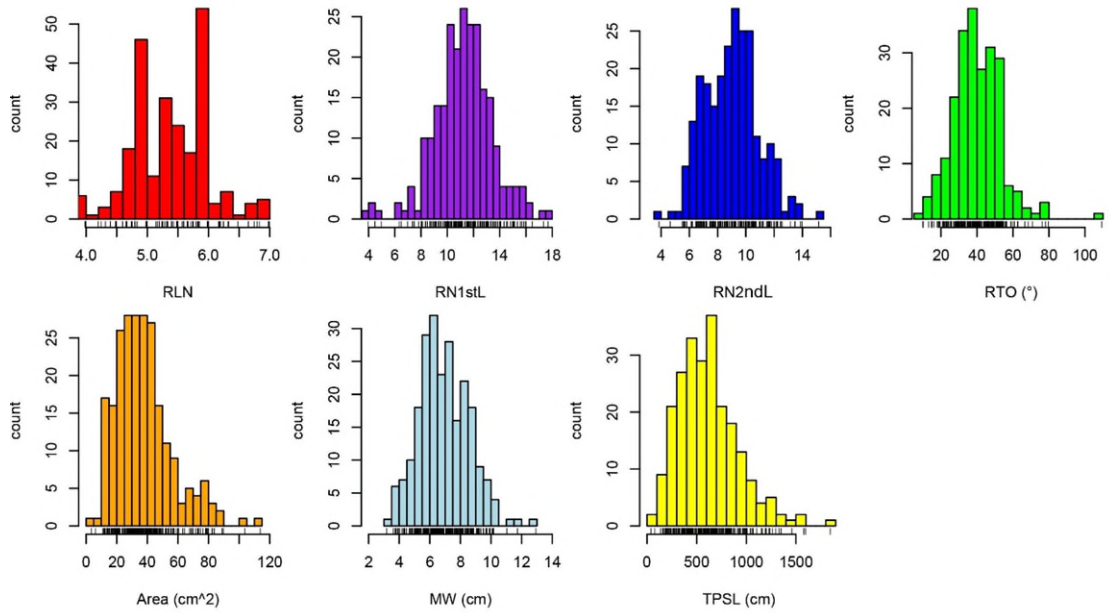

Fig. 1 histogram for seven root-related traits in a maize inbred association panel. RLN, root layer number; RN1stL, root number at the 1st layer; RN2ndL, root number at the 2nd layer; RTO, root angle opening; Area, area of all root; MW, maximum width; TPSL, total projected structure length.

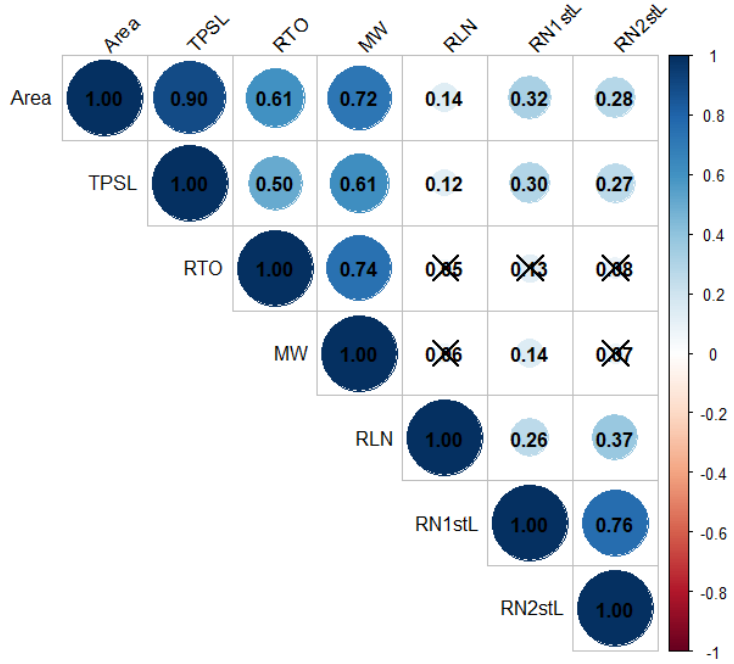

Fig. 2 correlation coefficients among seven maize root-related traits. Correlation coefficients marked with × are not significant; the remaining correlation coefficients are significant at $p < 0.05$. RLN, root layer number; RN1stL, root number at the 1st layer; RN2ndL, root number at the 2nd layer; RTO, root angle opening; Area, area of all root; MW, maximum width; TPSL, total projected structure length.

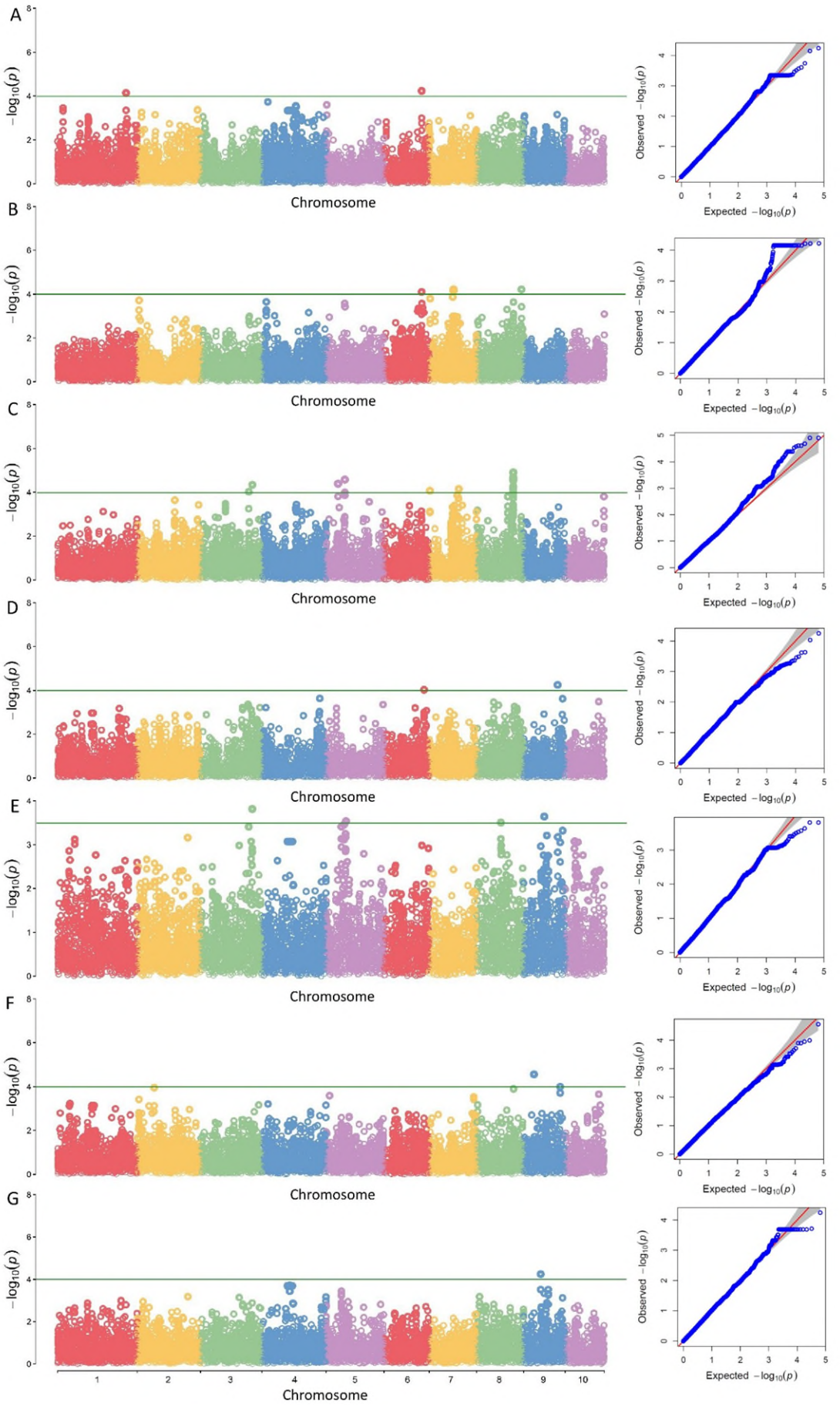
A
B
C
D
E
F
G
$-\log_{10}(p)$
Chromosome
Observed $-\log_{10}(p)$
Expected $-\log_{10}(p)$
1
2
3
4
5
6
7
8
9
10

Fig. 3 Manhattan plots and quantile–quantile (QQ) plots for root layers number (RLN, A), root number at the first layer (RN1stL, B), root number at the second layer (RN2ndL, C), root angle opening (RTO, D), area of all root derived pixels within the convex hull in cm^2 (Area, E), maximal width (MW, F), and total projected structure length (TPSL, G) in a maize inbred association panel

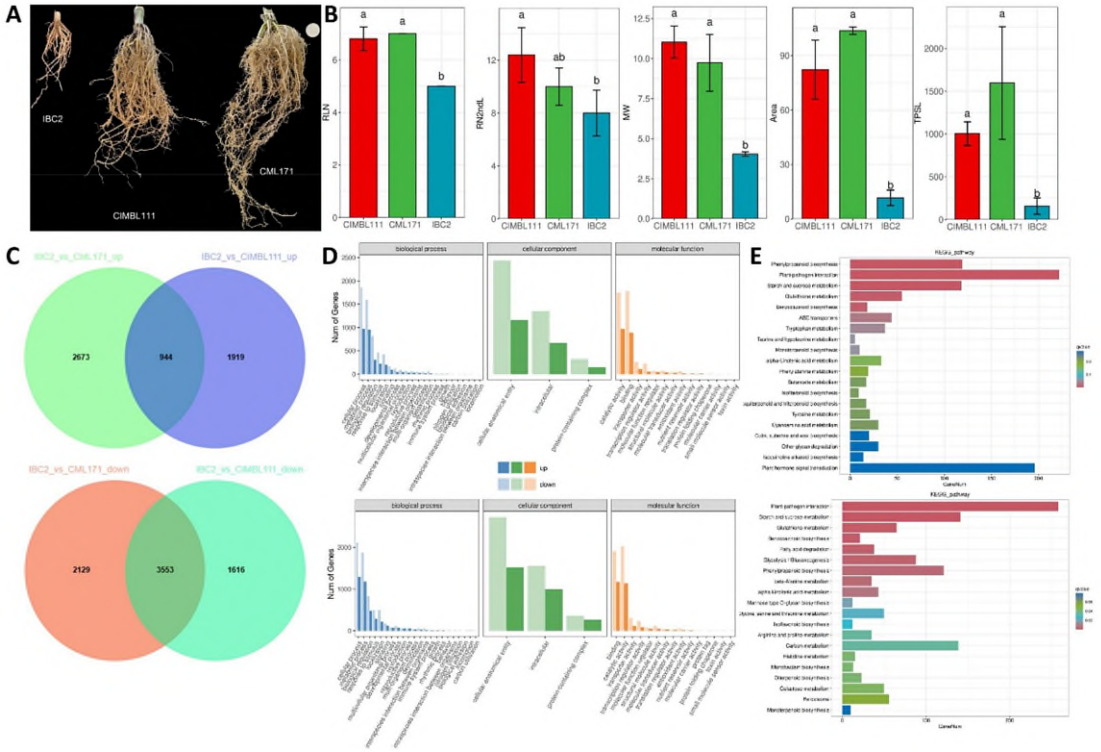

Fig. 4 Transcriptome analysis and KEGG pathway enrichment analysis in three inbred lines, CML171, CIMBL111, and IBC2. (A) Root architecture performance. (B) Comparison of root-related traits among CML171, CIMBL111, and IBC2, including root layer number (RLN), root number at the second layer (RN2ndL), area of all root-derived pixels within the convex hull (Area, cm^2), maximal width (MW), and total projected structure length (TPSL). (C) Number of differentially expressed genes (DEGs) between IBC2 and CML171, and between IBC2 and CIMBL111. "Up" and "Down" indicate genes up-regulated and down-regulated, respectively, in the shallow-root inbred line relative to the deep-root inbred line. (D) GO classification of differentially expressed genes between IBC2 and CIMBL111 (upper panel) and between IBC2 and CML171 (lower panel). (E) KEGG enrichment bar chart of differentially expressed genes between IBC2 and CIMBL111 (upper panel) and between IBC2 and CML171 (lower panel).

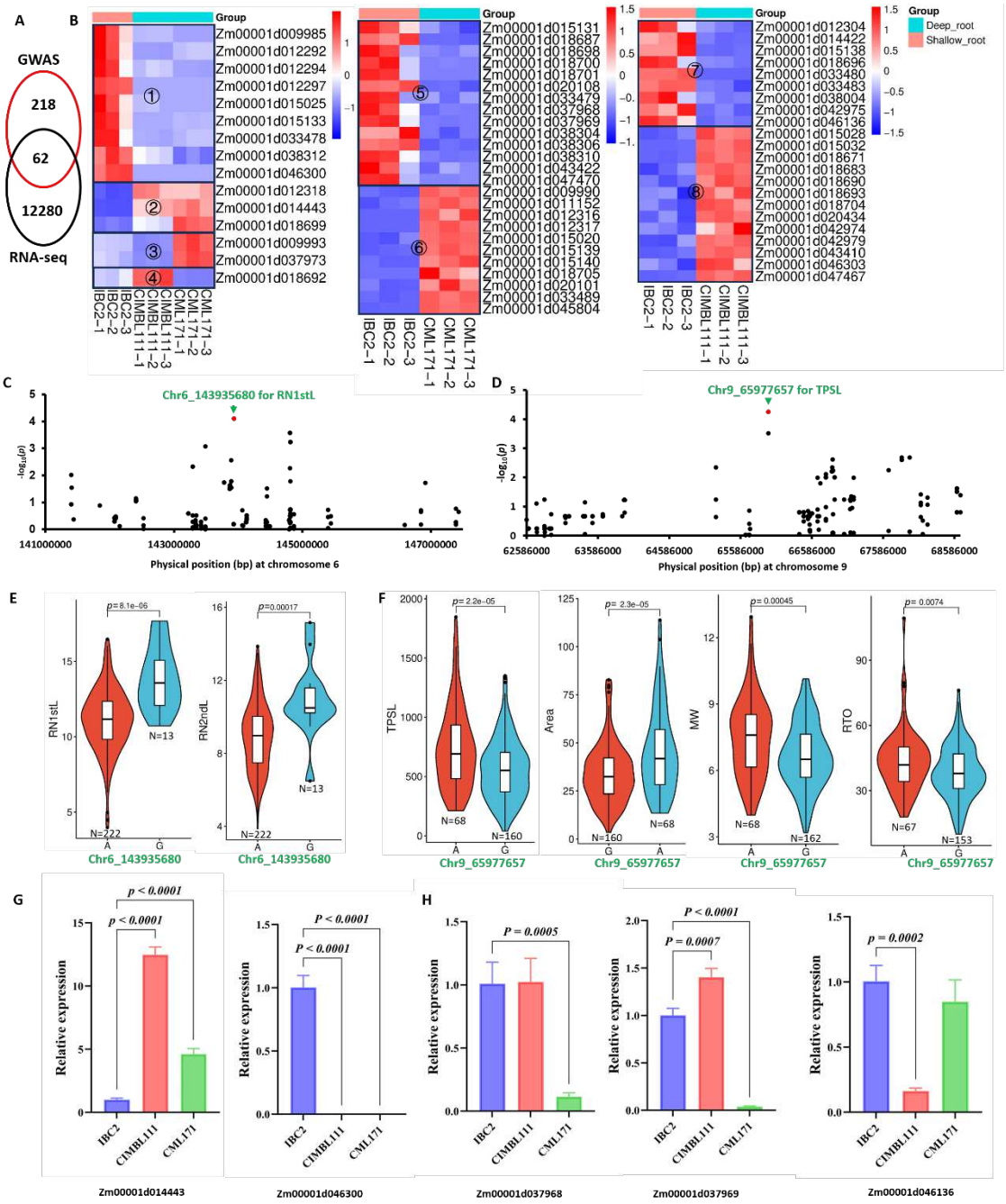

Figure 5 Integrated analysis of GWAS and RNA-seq for maize root system architecture traits and candidate gene identification. (A) Venn diagram showing the overlap between 218 candidate genes identified by GWAS and 12,280 differentially expressed genes (DEGs) identified by RNA-seq. The intersection contains 62 co-identified candidate genes. (B) Heatmap of expression patterns for the 62 candidate genes in the roots of a shallow-rooted inbred line, IBC2, and deep-rooted inbred lines CIMBL111 and CML171. The genes were clustered into eight groups (labeled ①-⑧). The color scale represents the normalized expression values (Z-score). (C) Manhattan plot for the most significant SNP Chr6_143935680 associated with root number at the 1st layer (RN1stL) on chromosome 6. (D) Manhattan plot for the most significant SNP Chr9_65977657 associated with total projected structure length (TPSL) on chromosome 9. (E) Phenotypic variations of RN1stL and root number at the 2nd layer (RN2ndL) among different alleles (A and G) at Chr6_143935680. (F)

Phenotypic variations of TPSL, root area (Area), maximum width (MW), and root angle opening (RTO) among different alleles (A and G) at Chr9_65977657. (G) Relative expression levels of candidate genes Zm00001d014443 and Zm00001d046300 in IBC2, CIMBL111, and CML171 evaluated by qRT-PCR. (H) Relative expression levels of candidate genes Zm00001d037968, Zm00001d037969, and Zm00001d046136 in IBC2, CIMBL111, and CML171 evaluated by qRT-PCR. Data in violin and bar plots are presented as mean ± SD, with *p*-values indicated.

Supplementary Files

This is a list of supplementary files associated with this preprint. Click to download.

- Figures.docx
- Tables.docx
- Supplementaryfigures.docx
- Supplementarytables.docx